# Non-polar organic compounds in autumn and winter aerosols in a typical city of Eastern China: Size distribution and impact of gas-particle partitioning on $PM_{2.5}$ source apportionment

Deming Han[1], Qingyan Fu[2], Song Gao[2], Li Li[3], Yingge Ma[3], Liping Qiao[3], Hao Xu[1], Shan Liang[1], Pengfei Cheng[4], Xiaojia Chen[1], Yong Zhou[1], Jian Zhen Yu[5], Jinping Cheng[1]

[1] School of Environmental Science and Engineering, Shanghai Jiao Tong University, Shanghai 200240, China

[2] Shanghai Environmental Monitor Centre, Shanghai 200235, China

[3] State Environmental Protection Key Laboratory of the Cause and Prevention of Urban Air Pollution Complex, Shanghai Academy of Environmental Science, Shanghai 200233, China

[4] School of Chemical and Environmental Engineering, Jiujiang University, Jiujiang 332005, Jiangxi, China

[5] Department of Chemistry, The Hong Kong University of Science and Technology, Hong Kong 999077, China

*Correspondence to*: Jinping Cheng (jpcheng@sjtu.edu.cn)

**Abstract**: Aerosol-associated non-polar organic compounds (NPOCs), including 15 polycyclic aromatic hydrocarbons (PAHs), 30 n–alkanes, 2 iso–alkanes, 5 hopanes and 5 steranes, were identified and quantified in $PM_{2.5}$ samples using thermal desorption–gas chromatography/mass spectrometry (TD-GC/MS) method. The samples were majorly collected in autumn and winter in a typical city of Eastern China. The total concentrations of NPOCs were 31.7–388.7 ng $m^{-3}$, and n–alkanes were the most abundant species (67.2%). The heavy molecular weight PAHs (4- and 5-ring) contributed 67.9% of the total PAHs, and the middle chain length n–alkanes ($C_{25}$–$C_{34}$) were the most abundant (72.3%) in n-alkanes. PAHs and n-alkanes were majorly distributed in 0.56–1.00 μm fraction, while ∑(hopanes+steranes) were associated with the 0.32–1.00 μm fraction, suggesting condensation of combustion products was their important origins. The ratio–ratio plots indicated that NPOCs in local area were affected by photochemical degradation. To reduce the uncertainty caused by only particle NPOCs data for source apportionment, the particle and predicted gaseous phases NPOCs, incorporated with other $PM_{2.5}$ compounds were used as input data for positive matrix factorization (PMF) model, respectively. Eight factors were extracted for both cases: secondary aerosol formation, vehicle exhaust, industrial emission, coal combustion, biomass burning, ship emission, dust and light NPOCs. These findings highlight the emissions from different aerosols associated NPOCs origins, caused different size-specific distributions, photo-degradation and gas-particle partitioning, which further affect $PM_{2.5}$ source apportionment. Considering these effects on organic tracers will help us accurately identify the potential sources of aerosols and then asses the contributions from each source.

## 1. Introduction

In recent years, severe atmospheric pollution characterized by haze has been occurring in developing countries, affecting visibility, optical radiation and human health (Yadav et al., 2013;Wang et al., 2015;Shen et al., 2015;Sulong et al., 2017). China has experienced numerous severe and long-lasting haze episodes since winter in 2013, which has affected over 600 million local residents and covered a quarter of the country's land area (Huang et al., 2014;Hao and Liu, 2015). In essence, haze episode is caused by the distribution of particle matters with different sizes in atmosphere, leading to decrease in visibility (Xie et al., 2017). Carbonaceous aerosols contain a large amount of particle matters, accounting for 30–50% of $PM_{2.5}$ mass concentrations (Yadav et al., 2013;Wang et al., 2016;Ma et al., 2018). Carbonaceous aerosols have significant influence on environmental and physical processes, including dry/wet deposition, cloud condensation nucleation, and heterogeneous reactions (Feng et al., 2006;Li et al., 2017).

Since carbonaceous aerosols can affect ambient environment significantly, it is crucial to investigate aerosol-associated organic compounds. Because non-polar organic compounds (NPOCs) can provide specific information on the identification of aerosol sources, they are now of special interest to researchers (Rajput and Sarin, 2014;Wang et al., 2016). n-Alkanes, polycyclic aromatic hydrocarbons (PAHs), hopanes and steranes are four typical NPOC species, and are frequently used to apportion sources of ambient particulate matters (Xu et al., 2013;Zhao et al., 2016). n-Alkanes are emitted from natural and anthropogenic activities, including particulate abrasion products from leaf surfaces of vegetation and fossil fuel combustion. Notably, fossil fuel combustion is characterized by the release of $C_{22}$–$C_{25}$ n-alkanes, while particulate abrasion products from leaf surfaces is characterized by the predominance of $>C_{29}$ odd n-alkanes (Yadav et al., 2013). PAHs are mainly emitted from anthropogenic activities, including biomass burning, coal combustion, fossil fuel combustion and industrial processes (Ma et al., 2011;Zhang et al., 2015). Hopanes and steranes are from unburned fossil fuels and lubricant oils, and they are often found in vehicle exhausts, ship emissions and coal combustion emissions.

PAHs are typical semi-volatile organic compounds, which can partition between gas and particle phases in ambient atmosphere (He and Balasubramanian, 2009; Ma et al., 2011). Recently, research has shown that n-alkanes, hopanes and steranes are also semi-volatile and subject to gas-particle partitioning (Xie et al., 2013;Xie et al. 2014;Wang et al., 2016). Additionally, another crucial factor affecting particle-bound concentrations of NPOCs is their aerodynamic diameter (Wang et al., 2009). The size-specific distributions of compounds are dependent on their physical-chemical properties, gas-particle partitioning and photodegradation (Okonski et al., 2014;Chen et al., 2016b). Thus, characterization of the size-specific distribution of NPOCs is crucial for understanding their formation, assessing their possible environmental

fate and offering proper management (Kleeman et al., 2008;Wang et al., 2009). Although several studies have focused on the size distribution of PAHs, much less attention has been given to other NPOC species (Hien et al., 2007;Wang et al., 2009).

NPOCs are typically assumed to be stable and nonreactive (Feng et al., 2006;Ma et al., 2011). However, recent research has shown that NPOCs can be oxidized by ·OH radicals, $RO_2$·radicals and $O_3$ over atmospherically relevant time scales (Xie et al., 2013;Wang et al., 2016). PAHs, n-alkanes, hopanes and steranes can undergo photochemical oxidation, increasing the production of secondary organic aerosol (Robinson et al., 2006;May et al., 2012). For example, PAHs can react with ·OH radicals, and through adding carbonyl groups to the carbon skeleton, the free ends of C-C scission products remain tethered together, which prevents fragmentation and leads to more functional groups on the single product (May et al., 2012). Hence, the low-volatility species which can condense into particle phase are formed, and subsequently undergo oligomerization reactions following condensation.

To develop strategies for controlling atmospheric pollution caused by particulate matter, receptor-based models (e.g., positive matrix factorization, PMF) have been widely applied to quantitatively apportion sources of particulate matter (Wang et al., 2009;Li et al., 2016;Huang et al., 2017). However, the output factors of receptor model are not necessarily emission sources, because there exist some atmospheric processes like photodegradation or gas-particle partitioning. Considering the gas-particle partitioning of NPOCs, Xie et al. (2013) adopted both gaseous and particulate NPOCs in PMF model and successfully extracted seven factors. More recently, Wang et al. (2016) used data of NPOCs combined with those of organic/elemental compounds (OC/EC), inorganic compounds and elemental compounds as input for PMF model, and they found that total (gas + particle) bound concentrations enabled more reasonable source profiles than single particle phase.

In this paper, we conducted a comprehensive study on $PM_{2.5}$-associated NPOCs in a typical city of Eastern China. Specifically, we: (1) quantified the concentrations of NPOCs (n–alkanes, PAHs, hopanes and steranes) through thermal desorption–gas chromatography/mass spectrometry (TD–GC/MS) method; (2) determined the size-specific distributions of NPOCs from 0.01 to 18 μm; (3) analyzed the degradation of NPOCs; (4) explored the gas-particle partitioning of NPOCs and assessed its effects on $PM_{2.5}$ source apportionment.

## 2. Materials and methods

### 2.1 Sampling sites and sample collection

Jiujiang city is located in 113°57'–116°53' E and 28°47'–30°06' N with elevation of 32 m in Jiangxi Province of Eastern

China (Fig. 1). It is characterized by a subtropical monsoon climate. Jiujiang is the second largest city in Jiangxi Province, with approximately 4.83 million resident population and over 700 thousand motor vehicles in 2015. Preliminary statistics indicate that the gross industrial standard coal consumption in Jiujiang amounted to 7.80 million tons in 2015. In Jiujiang, petrochemical industry, which can process approximately five million tons of crude oil per year, is located at the northeast part of the city and in upwind direction. In addition, Mount Lu (elevation of 1474 m), located at the south of Jiujiang, blocks the transport of air masses from Northern China Plain region to southern area, leading to the accumulation of particulate matters in the city area, especially in winter seasons.

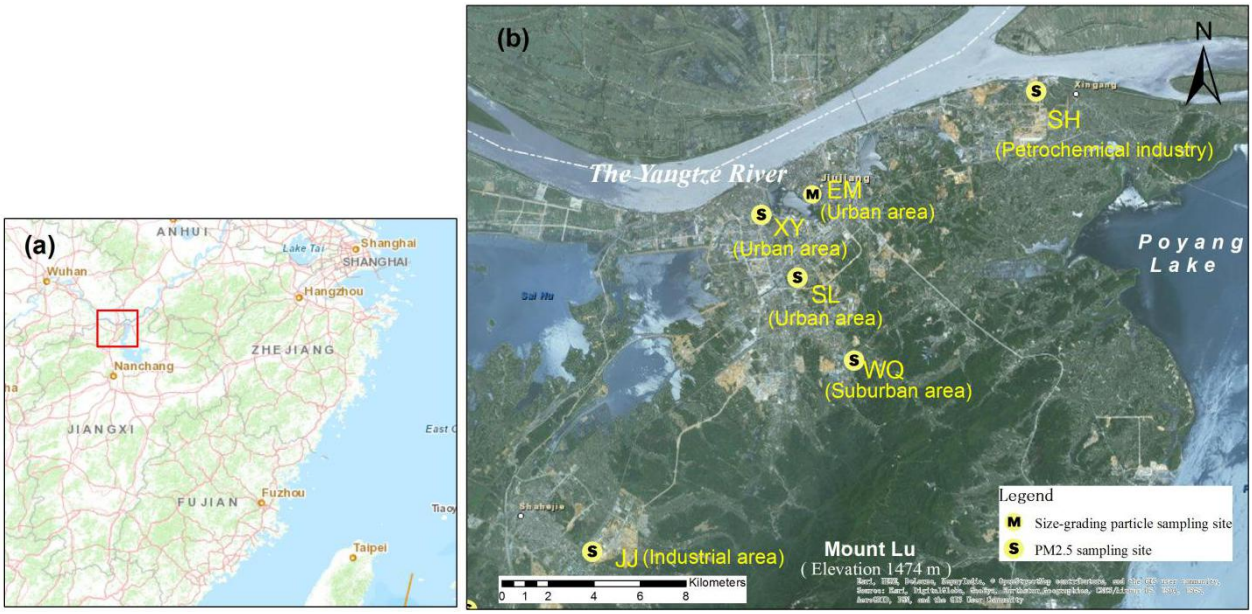


**Fig. 1.** Location of aerosol sampling sites in Jiujiang City, Eastern China

Five $PM_{2.5}$ sampling sites were selected for routine air quality measurements in Jiujiang city (Table 1), including Shihua (SH), Xiyuan (XY), Shili (SL), Wuqierqi (WQ) and Jiujiangxian (JJ). All $PM_{2.5}$ filter samples were collected using medial-volume air samplers (YH-5, Qingdao, China), at a flow rate of 100 L $min^{-1}$. Particles were collected on quartz fiber filters (GE Whatman, 1851-090, England, UK) with a diameter of 90 mm, each for a duration of 23 h. Prior to use, these filters were prebaked at 550 °C for 4 h to eliminate residual organic compounds. $PM_{2.5}$ sampling at these five sites were performed synchronously for five continuous days per month from Sep. to Dec. 2016, in addition to the extensive sampling period (Dec. 1–16). A total of 137 $PM_{2.5}$ valid samples were collected, as 18 samples were invalid or missing due to the bad weather or power problems during sampling period.

107 **Table 1.** Detailed description of the six sampling sites in this study

| Site | Type | Surrounding area | Height | Main pollutants | Sampling time |
|---|---|---|---|---|---|
| SH | Residential area | 1.7 km to petrochemical industry; 600 m to traffic road | ~12 m | Petrochemical industry | Sep. 9-13; Oct. 11-15; Nov. 10-14; Dec. 1-16 |
| XY | Urban area | 500 m to traffic road; 1 km to wharf | ~23 m | Vehicle; ship | Sep. 9-13; Oct. 11-15; Nov. 10-14; Dec. 1-16 |
| SL | Urban center | 500 m to traffic road | ~20 m | vehicle | Sep. 9-13; Oct. 11-15; Nov. 10-14; Dec. 1-16 |
| WQ | Suburban area | 1.3 km to the city center | ~17 m | vehicle | Sep. 9-13; Oct. 11-15; Nov. 10-14; Dec. 1-16 |
| JJ | Industrial area | Located in industrial area; 500 m to highway | ~20 m | Industry emission | Sep. 9-13; Oct. 11-15; Nov. 10-14; Dec. 1-16 |
| EM | Urban area | 500 m to traffic road | ~20 m | vehicle | Dec. 1-16 |

108

109 The sampling site of size–specific aerosols was located at a five–story building of Jiujiang Environmental Monitor
110 Station (EM site). Airborne particle samples were collected for 23 h using a Nano–Micro–orifice Uniform Deposition
111 Impactor (MOUDI) sampler (Model 122R, MSP Cor, USA), at air flow rate of 30 L/min. Detailed instrument operation,
112 quality assurance and control method can be found in our previous work (Chen et al., 2016b;Han et al., 2018). Briefly,
113 this sampler can collect particles within 13 size fractions: 0.01–0.018, 0.018–0.032, 0.032–0.056, 0.056–0.1, 0.1–0.18,
114 0.18–0.32, 0.32–0.56, 0.56–1.0, 1.0–1.8, 1.8–3.1, 3.1–6.2, 6.2–9.9, 9.9–18 μm. Prior to sampling, each filter tray was
115 washed with distilled water and ethanol. Two kinds of quartz fiber filters of diameters of 47 and 90 mm were used to
116 collect particles with diameter of 0.056-18.0 and 0.010-0.056 μm, respectively. All the filters were prebaked at 550 ºC for
117 4 h, wrapped in aluminum foil and then sealed in clean polyethylene bags. Leak and flow tests were conducted according
118 to manufacturer's instructions: leak test was done with a duration of 60 s with leak rate < 10 Pa/s at initial pressure of
119 55±5 kPa. The mass concentrations of particle matters were determined by subtracting the filter weight before and after
120 sampling. A well calibrated digital balance within a precision of 0.01 mg (Sartorius SE2, Germany) was used. The
121 collected particle samples were stored at controlled temperature (–20 ºC) and relative humidity until analysis.

122 **2.2 Analysis of aerosol samples using TD–GC/MS**

123 Fifty-seven NPOC species (Table S1 and Fig. S1 in Supplementary Materials) were identified by using an in-injection
124 port thermal desorption union (TDU, Shimadzu, Japan), coupled with gas chromatography/mass spectrometer (GC/MS,
125 QP2010 Plus, Shimadzu, Japan). Compared with traditional solvent extraction method, TD–GC/MS method (Ho and Yu,
126 2004;Ho et al., 2008) has advantages such as solvent and sample filtration, labor saving, and less contamination from
127 solvent impurities. A filter aliquot (1 $cm^2$) from quartz fiber was cut into small pieces on a clean glass dish, and then they

were inserted into the TD tubes (CAMSCO, USA). Both sides of the samples were surrounded with pre-baked, silane-treated glass-wool plugs, to enhance the cryofocusing of the analytes and prevent heavy and polar compounds from entering the GC column. The internal standards of n–tetracosane $d_{50}$ (n–$C_{24}D_{50}$), naphthalene–$d_8$, acpnaehthene–$d_{10}$, phenanthrene–$d_{10}$, and chrysene–$d_{12}$ were spiked into each sample, through a pipette with a long thin tip. This was done to account for the loss of components from sample filters associated with the instrument instability due to changes in laboratory environmental conditions. After the evaporating of solvent from internal standard was conducted via air drying for several seconds, the TD tubes were capped and put into a sampler holder.

The sample processing time in TD tube was set to 45 min, and the TD tube was electronically cooled to −10 ºC. The desorption and interface temperatures were set to 295 and 280 ºC, respectively. Helium (99.999%) was used as carrier gas for the thermally desorbed organic compounds, with gas flow rate of 1.12 mL/min. GC was used under splitless injection mode, and the initial oven temperature was set to 40 ºC with an isothermal hold time of 5 min. Stepwise programmed linear temperature ramping included 10 ºC/min to 120 ºC (held for 2 min), and then 20 ºC/min to 300 ºC (kept for 20 min). A Rtx–5MS capillary column (Restek, USA, L × I.D. 30 m × 0.25 mm, df 0.25 μm) was used to separate desorbed organic compounds. The MS was operated in scan mode with mass range was m/z 50–500, and scanned at 0.5 s/scan (Ho et al., 2008;Yadav et al., 2013). The ion was produced from electronic impact ionization (EI) at 70 eV, and then was separated by high performance quadrupole mass filter. Species identification was achieved via comparing the mass spectra and retention times of the chromatographic peak with the corresponding authentic standards.

### 2.3 Determination of OC/EC and other constituents

OC and EC were analyzed (a round punch of 0.538 $cm^2$) using the thermal–optical– transmittance (TOT) method (NIOSH protocol, Desert Research Institute, USA) (Han et al., 2018). The instrument included a temperature- and atmosphere-controlled oven and a laser of 680 nm wavelength to generate an operational EC/OC split. The instrument was heated stepwise from start to 250 ºC (60 s), 500 ºC (60 s), 650 ºC (60 s) and finally 850 ºC (90 s) in the helium atmosphere for OC volatilization, and from start to 550 ºC (45 s), 650 ºC (60 s), 750 ºC (60 s) and finally 850 ºC (80 s) in the helium atmosphere containing 2% oxygen for EC oxidation.

Elemental compositions, including Na, K, Ca, Mg, P, Fe, Ti, Al, Pb, Cu and Zn, were determined by energy dispersive X-ray fluorescence (ED-XRF) spectrometry (Epsilon 5, Netherlands). Water soluble inorganic ions, including cations ($Na^+$, $K^+$, $Mg^{2+}$, $Ca^{2+}$, $NH_4^+$) and anions ($Cl^–$, $SO_4^{2–}$ and $NO_3^–$, $NO_2^-$), were detected by ion chromatography (IC, ISC-90, Dionex, USA). The detailed experimental procedure of OC/EC, elemental composition, inorganic ions analysis could be found in Li et al. (2017) and Han et al. (2018).

157 **2.4 Quality assurance and quality control**

158 Prior to sampling in each site, the five $PM_{2.5}$ samplers were calibrated by environmental monitor station. $PM_{2.5}$ samplers
159 were placed on the building rooftop of Jiujiang Environmental Monitor Station, each two within distance of <3 m. Field
160 blanks were collected by keeping blank filters in the sampler for the same duration at sampling site. Additionally, both
161 transport and laboratory blank filters were analyzed, and all the data reported in this study were corrected according to
162 the results.

163 The NPOCs standards used were National Institute of Standards and Technology (NIST, USA) Standard Reference
164 Materials (SRM), including SRM 2260A, SRM 1494 and SRM 2266 for 15 PAHs, 30 n-alkanes and 10 hopanes/steranes,
165 respectively. Six–point calibration curves of NPOCs were constructed through adopting different calibration
166 solutions, namely 0, 0.05, 0.25, 0.50, 1.0 and 2.0 μg $L^{-1}$ for PAHs, hopanes and steranes, while 0, 0.10, 1.0, 5.0, 10.0
167 and 20.0 μg $L^{-1}$ for n–alkanes, to the field blank filters and loaded into TD tubes._The same concentration of internal
168 standards were used for each level of calibration solution. Ratios of the average peak area values 'A' for represented
169 samples 'S' to the corresponding internal standard 'IS', namely AS/AIS; and ratios of average concentration 'C' for
170 represented samples to the corresponding internal standard (CS/CIS), were generated via using Shimadzu software
171 with the slope of the curve being the RRF (relative response factor). The calibration curves for most target
172 compounds were highly linear ($r^2$>0.99), demonstrating the consistency and reproducibility of this method. The
173 standard deviation (S) was calculated by using seven replicates of the second lowest standard solution, and the
174 method detection limit (MDL, MDL =3.143×S) was determined at the 99% confidence level.

175 Recovery experiment were conducted to improve the desorption of targeted compounds from filters and
176 experimental detection. The analytical recovery was calculated via spiking a known amount of the SRM solution to
177 blank filter, and most compounds were recovered with recovery efficiency >90% except for several light molecule
178 weight species. The accuracy of the method was evaluated by reproducibility of the standard and selected samples
179 ascertained by processing in quintuplicate, and results suggest the analytical precision was better than 5%.

180 **2.5 Diagnostic parameters and isomeric ratios**

181 Different diagnostic parameters were adopted in this study to explore natural and anthropogenic contributions. The
182 parameters include carbon preference index (CPI), the carbon number of the most abundant n–alkane ($C_{max}$),
183 contributions from natural wax n–alkanes (WNA%) and petrogenic n–alkanes (PNA%), higher plant n–alkane average
184 chain length (ACL), and molecular diagnostic ratios (MDRs) for PAHs (Yadav et al., 2013;Zhao et al., 2016).

185 (1) CPI is defined as the ratio of the total concentration of odd n–alkanes to that of even n–alkanes (Eq. (1)). It reflects

the comparison between natural and anthropogenic contributions.

$$CPI = \frac{\sum_{i=11}^{39} C_i}{\sum_{j=12}^{40} C_j} \quad (1)$$

where i and j represent odd and even carbon numbers, respectively, and C represent the concentrations of carbon n–alkanes.

(2) WNA% is calculated as Eq. (2). Note that negative value of $[C_i – (C_{i–1} + C_{i+1})/2]$ was replaced by zero.

$$WNA\% = \frac{\sum WNA_{Cn}}{\sum NA_{Cn}} = \frac{\sum_{i=11}^{39} [C_i - (C_{i-1} + C_{i+1})/2]}{\sum_{n=11}^{40} C_n} \quad (2)$$

(3) Aerosol-associated n–alkanes can originate from plant wax or petroleum combustion, and the percentage of petrogenic n–alkanes (PNA%) can be calculated as:

$$PNA\% = 100\% - WNA\% \quad (3)$$

(4) $C_{max}$ represents the carbon number of the most abundant n–alkane, and it is regarded as the most important indicator of biogenic inputs. In general, $C_{max}$ = 31 indicates effects from leaf abrasion products, whereas $C_{max}$ = 29 implies effects from road dust, as well as vehicle and industrial emissions.

(5) ACL can indicate emissions of n–alkanes from plants which are related to temperature and humidity. It is defined as counted carbon atoms per carbon molecule, depending on the odd n–alkanes from higher plant. ACL can be estimated through Eq. (4) as follows:

$$ACL = \frac{23 \cdot C_{23} + 25 \cdot C_{25} + \cdots + 39 \cdot C_{39}}{C_{23} + C_{25} + \cdots + C_{39}} \quad (4)$$

(6) MDRs for PAHs source apportionment include ANT/PHE (Anthracene/Phenanthrene) ratio, PYR/FLU (Pyrene/Fluoranthene) ratio, IcdP/BghiP (Indeno[1,2,3-cd]pyrene/Benzo[ghi]perylene) ratios (namely, ANT/(ANT+PHE) ratio and FLU/(FLU+PYR) ratio), and IcdP/(IcdP+BghiP). If ANT/(ANT+PHE) < 0.1, petroleum origins are suggested; if the ratio > 0.1 pyrogenic sources are indicated. If FLU/(FLU+PYR) < 0.4, petroleum sources are suggested; if the ratio > 0.4, pyrogenic sources are indicated (Kuang et al., 2011;Chen et al., 2016a). Note that the ratio ranging from 0.4 to 0.5 also suggests fuel combustion. If 0.2 < IcdP/(IcdP+BghiP) < 0.5, fuel combustion is suggested; if the ratio > 0.5, grass, wood and coal combustion should have contributed to particulate matters (Chen et al., 2016a).

### 2.6 Gas-particle partitioning model

Gas-particle partitioning is an important mechanism that affects the fate and transport of NPOCs (Pankow, 1994;Kim et al., 2011). To understand the partitioning behavior of NPOCs, we evaluated the distribution of NPOCs between gas and particle phases in the atmosphere. The gas-particle coefficient $K_p$ ($m^3$ $\mu g^{-1}$) for each compound species was calculated

using the following equations:

$$K_p = \frac{F/PM}{A} = \frac{R \cdot T}{10^6 \cdot MW_{OM} \cdot \xi_{OM} \cdot P_L^o} \quad (5)$$

$$P_L^o = P_{L,0}^o \cdot \exp\left[\frac{\Delta H_0}{R}\left(\frac{1}{298} - \frac{1}{T}\right)\right] \quad (6)$$

where F and A represent the concentrations of NPOC in gas and particle phases (ng $m^{-3}$), respectively; PM is the measured mass concentration of particulate matter, *i.e.*, $PM_{2.5}$ in this study (μg $m^{-3}$); R is the ideal gas constant (8.314 $m^3$ $Pa^{-1}$ $K^{-1}$ $mol^{-1}$); T is the ambient temperature (K); $MW_{OM}$ is the mean molecular weight (g $mol^{-1}$), and is 200 g $mol^{-1}$ in this study (Xie et al., 2013); $\xi_{OM}$ is the activity coefficient of each compound in the absorbing phase and assumed to be unity in this calculation (Xie et al., 2013); $P^o_L$ and $P^o_{L,0}$ are subcooled vapor pressures at T and 298 K, respectively (Pa); $\Delta H_0$ is vaporization enthalpy of the liquid at 298.15 K. The measured $P^o_L$ and $\Delta H_0$ were extracted from previous literatures (And and Hanshaw, 2004;Wang et al., 2016).

The total concentration (S) of each NPOC in gas and particle phases was calculated as Eq. (7):

$$S = F + A = \left(1 + \frac{10^6 \cdot MW_{OM} \cdot \xi_{OM} \cdot P_L^o}{R \cdot T \cdot PM}\right) \times F \quad (7)$$

Also, Jungle–Pankow model was further used to investigate gas-particle partitioning. In this model, the ratio (φ) of the concentration of NPOC species in particle phase to the total NPOC concentration was calculated:

$$\varphi = \frac{C_p}{C_p + C_g} = \frac{c \cdot \theta}{c \cdot \theta + P_L^o} \quad (8)$$

$$\log Kp = \log\frac{c \cdot \theta}{PM} - \log P_L^o \quad (9)$$

where θ represents particle surface area per unit volume of air ($cm^2$ $cm^{-3}$) and c is a constant which depends on thermodynamics of the adsorption process, molecular weight, and surface properties (Pa $cm^{-1}$). In this study, c = 17.2 Pa $cm^{-1}$, and θ is $1.1\times10^{-5}$, $1.5\times10^{-6}$ and $4.2\times10^{-7}$ ($cm^2$ $cm^{-3}$) for urban area, rural area and background, respectively (And and Hanshaw, 2004; Xie et al., 2013).

## 3. Results and discussion

### 3.1 Abundance of $PM_{2.5}$ and NPOCs

The statistical summary and the abundance of measured $PM_{2.5}$ and NPOC species are shown in Fig.2 and Table S2. The daily average $PM_{2.5}$ concentration in all sampling sites was 79.3±37.7 μg $m^{-3}$. The average OC and EC concentrations were 13.8±6.9 and 6.3±2.2 μg $m^{-3}$, respectively. Organic matter (OM) was estimated to be 1.4 times of OC concentration

238 (Feng et al., 2006;Huang et al., 2014), which was the most abundant component in $PM_{2.5}$, accounting for 18.8–27.8% of
239 the total mass in this study. Following OM, $NO_3^-$, $SO_4^{2-}$ and $NH_4^+$ were also abundant, accounting for 19.9–22.6%,
240 16.4–18.1% and 10.4–13.7% of $PM_{2.5}$, respectively.

241 Fifty-seven NPOCs were identified in this study (Table 2), including 30 n-alkanes, 2 iso-alkanes, 15 PAHs, 5 hopanes
242 and 5 steranes. Their daily average concentrations ranged from 31.7 to 388.7 ng $m^{-3}$ (an average of 155.9±55.4 ng $m^{-3}$),
243 accounting for 0.4–2.4% of OM. This was consistent with the measurement results (0.1–4.2%) of NPOCs in Pearl River
244 Delta (PRD, China) (Wang et al., 2016), over a two-year period from 2011 to 2012. Similarly, Zhao et al., (2016) found
245 that the NPOCs varied from 19.8 to 288.2 ng $m^{-3}$, accounted for 0.8–1.7% of OM in South China Sea from Sep. to Oct.
246 2013. n-Alkanes were the most abundant NPOCs, with concentration of 105.3±55.1 ng $m^{-3}$, accounting for 67.2% of
247 NPOC concentration. PAHs was the second most abundant species, averagely accounting for 29.2% of NPOC
248 concentration. Hopanes and steranes were minor constituents, with average concentrations of 3.6±3.0 and 1.8±1.3 ng $m^{-3}$,
249 respectively.

250 When comparing with other NPOCs measurements in China, Li et al. (2013) reported a comparable level that the daily
251 concentration of n-alkanes, PAHs and hopanes were 97.9, 13.5 and 21.5 ng $m^{-3}$ in Hong Kong in winter, respectively. Xu
252 et al. (2013) measured mean n-alkanes, PAHs concentrations of 48.1±20.8, 19.0±17.5 ng $m^{-3}$ in urban Guangzhou during
253 16$^{th}$ Asian Games, while Feng et al. (2006) found that the daily concentrations of n-alkanes, PAHs ranged of 32.9–342.9
254 and 7.8–151.1 ng $m^{-3}$ in urban Shanghai in 2002–2003, respectively. Thus, this study finds generally higher $PM_{2.5}$
255 associated NPOCs concentrations measured in Jiujiang compared to other measurements, which may be due to this study
256 was mainly conducted in cold season when severe atmospheric pollution episodes (including haze) frequently occurred.
257 In addition, aerosols and NPOCs would transported to Jiujiang from Northern China where has significant amounts of
258 coal burned and industries, through long range transport of air mass (Han et al., 2018). However, the annual average
259 concentrations of $PM_{10}$ bound n-alkanes and PAHs in Delhi, India (Yadav et al., 2013) were 4.0 and 8.2 times higher than
260 that in Jiujiang, respectively.

261 **Table 2.** Comparison of NPOC concentrations between Jiujiang City and other areas (ng $m^{-3}$)

| | n-Alkane [a] | PAHs [b] | Hopane [b] | Sterane [b] | Time | Reference |
|---|---|---|---|---|---|---|
| Jiujiang, China | 105.3±55.1 (16.3–305.0); $C_{11}$–$C_{40}$ | 45.3±17.6 (12.3–96.5); 15 | 3.6±3.0 (0.6–16.4); 5 | 1.8±1.3 (0.3–7.0); 5 | 2016.9–12 | This study |
| Shanghai, China | 32.9–341.9; $C_{17}$–$C_{36}$ | 7.8–151.1; 15 | / | / | 2002–2003 | Feng et al., 2006 |
| Beijing, China | 163.0±193.5; $C_{20}$–$C_{35}$ | 78.7±115.4; 16 | 6.9±6.6; 4 | / | 2004 | Feng et al., 2006 |
| Guangzhou, China | 48.1±20.8; $C_{19}$–$C_{40}$ | 19.0±17.5; 18 | / | / | 2010.11 | Xu et al., 2013 |
| South China Sea | 15.7–124.2; $C_{15}$–$C_{38}$ | 3.4–127.9; 22 | 0.4–19.6; 8 | 0.4–3.5; 6 | 2013.9–10 | Zhao et al., 2016 |
| Hong Kong, China | 97.9; $C_{29}$–$C_{33}$ | 13.5; 15 | 21.5 | / | 2003,11-12 | Li et al., 2013 |

| | | | | | | |
|---|---|---|---|---|---|---|
| Pearl River Delta | 1.6–436(64); | 0.1–74(14.2); 17 | 0.3–21(2.3); | 0.01–4.1(3.4 | 2011–2012 | Wang et al., 2016 |
| [c], China | $C_{22}$– $C_{38}$ | | 10 | );5 | | |
| British Columbia | 4.89–74.38(15.58); | 1.01–41.7 | / | / | 2005.12–2 | Ding et al., 2009 |
| Canada | $C_{11}$–$C_{40}$ | (10.82); 16 | | | 007.2 | |
| Delhi, India | 425±343; $C_{12}$–$C_{35}$ | 373±197; 17 | / | / | 2006–2009 | Yadav et al., 2013 |

[a]: mean concentration (concentration range); species;

[b]: mean concentration (concentration range); number of species;

[c]: including four cities in Pearl River Delta: Guangzhou, Dongguang, Nanhai and Nansha.

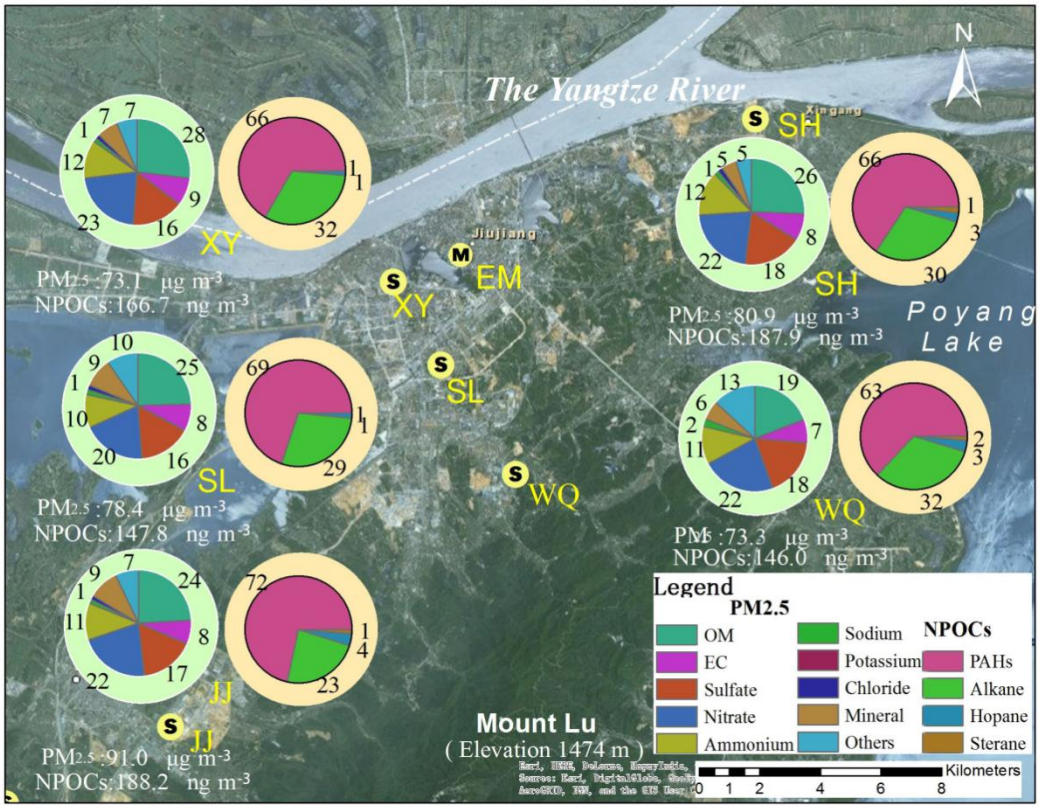


**Fig. 2.** The percentiles of NPOCs and $PM_{2.5}$ constituents in five sampling sites in Jiujiang city

### 3.1.1 PAHs

PAHs are ubiquitous pollutants of the environment. They are originated from natural and anthropogenic sources such as biomass burning, vehicle exhausts, residential heating, waste incineration and industrial emissions. The $PM_{2.5}$-associated PAHs were shown in Fig. 3a. Their individual species concentrations varied between 0.4 and 5.7 ng $m^{-3}$. BbF (Benzo[b]fluoranthene, 5.7 ng $m^{-3}$) was the most abundant PAH species, followed by BaA (Benz[a]anthracene, 5.6 ng $m^{-3}$) and BaP (Benzo[e]pyrene, 4.2 ng $m^{-3}$), together accounting for 34.2% of all PAHs, this was consistent with some previous studies in Guangzhou (Xu et al., 2013). Because of the strong carcinogenic effect of BaP, special attention should be given to it, the level of which was also higher than that indicated by the air quality guideline of WHO (1 ng $m^{-3}$).

Due to the vapor pressure dependent partitioning, 2- and 7–ring PAHs distributed majored in gas and particle phases, respectively. However, PAHs with 3–6 rings appeared in both gas and particle phases through gas-particle partitioning. Moreover, FLU–PYR–CHR (Chrysene) and BaA–BaP congeners of the 4–ring PAHs often indicate diesel vehicle and biomass combustion (Yadav et al., 2013), respectively, while 5–ring BkF is considered as marker of vehicle tracer. The total percent contribution of 4– and 5– ring PAHs was 67.9% in this study, suggests vehicle exhaust, biomass burning and fossil fuel combustion have mixed effects on local atmospheric pollution.

MDRs of atmospheric PAHs with similar molecular weight have been widely used as a useful tool for aerosol source identification. In this study, the ANT/(PHE+ANT) ratios varied in 0.28–0.68 (mean of 0.48), which were bigger than 0.1 confirming a strong influence from pyrogenic emissions (Xu et al., 2013;Yadav et al., 2013). Most samples had FLU/(FLU+PYR) ratios of 0.36–0.58, implying combined effects of pyrogenic emission and combustion of fuel, grass, wood and coal (Kuang et al., 2011;Chen et al., 2016a). The average IcdP/(IcdP+BghiP) ratio was 0.57, and in most cases the ratio > 0.50, suggesting significant impacts from the combustion of grass, wood and coal. Despite MDRs have been consistently used for PAHs source identification, it remains a rather rough method and contradictions may occur sometime. Therefore, more samples should be collected to achieve better results.

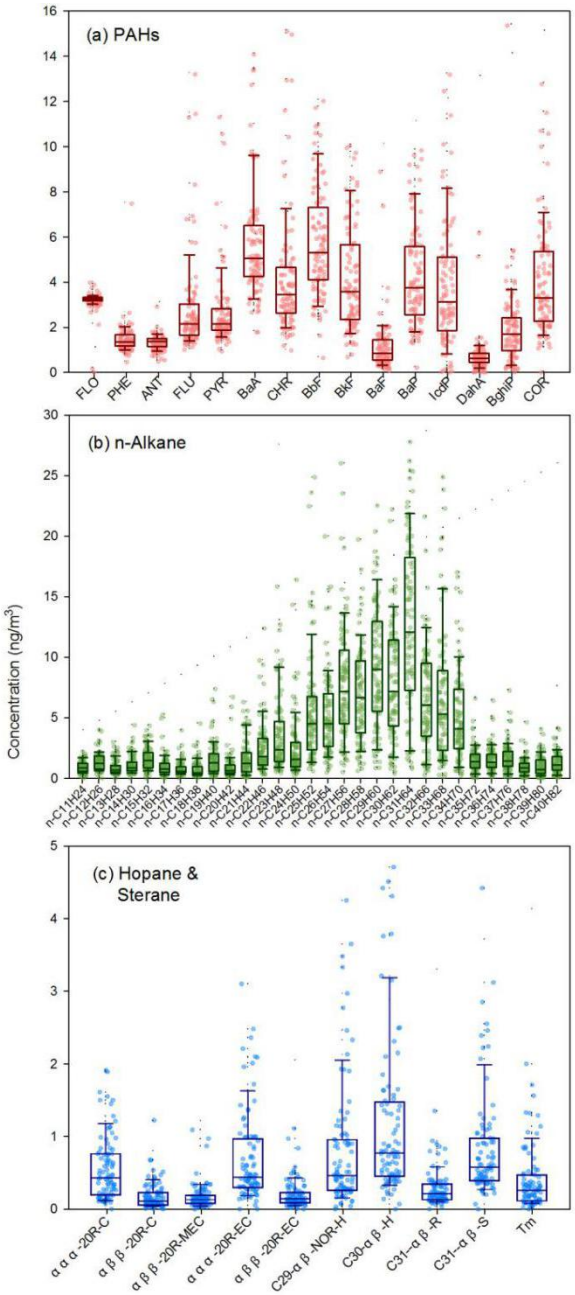


**Fig.3.** Concentration profiles of NPOCs

### 3.1.2 n-Alkanes

Unique signatures of n-alkanes have been shown for different sources, including vehicle exhausts, tire-wear particles, road dust, cooking oil, cigarette smoke and particulate abrasion products from leaf epicuticular waxes (Rogge et al., 1994;Ma et al., 2011;Yadav et al., 2013;Zhang et al., 2015). A bimodal distribution of chain lengths of n-alkanes with peaks at $C_{20}$–$C_{22}$ and $C_{24}$–$C_{27}$ implies vehicle exhaust sources (Zhang et al., 2015). However, a unimodal distribution of chain lengths of >$C_{30}$ n–alkanes (peak at $C_{37}$) represents tire-wear particle sources. The distribution pattern characterized by large proportion of $C_{27}$–$C_{33}$ odd n–alkanes suggests vegetation sources.

Our analysis showed that the middle-chain-length n-alkanes ($C_{25}$–$C_{34}$) were the most abundant (Fig. 3b), accounting for 72.3% of the total measured n-alkanes. Feng et al. (2006) and Xu et al. (2013) reported similar findings that $C_{27}$–$C_{29}$ n-alkanes dominated the distribution of n-alkanes in three metropolitan cities of China (Beijing, Shanghai, Guangzhou). In addition, a predominance of odd carbon numbered congeners ($C_{25}$, $C_{27}$, $C_{29}$, $C_{31}$ and $C_{33}$) was found, with $C_{max}$ = 31 in most cases and $C_{max}$ = 29 in a few cases (Fig. 3b). The $C_{max}$ value in this study suggests that emissions arising from leaf abrasion products contributed to n-alkanes concentrations in Jiujiang city. However, no obvious odd/even carbon preference was observed for either $C_{11}$–$C_{14}$ nor $C_{35}$–$C_{40}$ n–alkanes.

Plant wax n-alkanes exhibit strong odd/even carbon number predominance, while n-alkanes from fossil fuel combustion do not (Feng et al., 2006). Thus, biogenic n-alkanes should have CPI values greater than unity, whereas anthropogenic n-alkanes should have CPI values close to unity. Furthermore, CPI < 2 is a typical characteristic of urban environment, suggesting major contribution from petrogenic sources, e.g., vehicle exhausts and industrial emissions. The CPI values were 1.00–1.79 (average of 1.29) in this study, implying strong contributions from petrochemical sources, diesel residues and gasoline emissions. Ding et al. (2009) reported a mean CPI value of 1.5 in central British Columbia of Canada, and Xu et al. (2013) reported CPI values of 1.2–1.7 (mean of 1.4) in Guangzhou of China. The mean contribution of plant wax n-alkanes to the total n-alkanes (WNA%) was 17.00±4.41%, ranging from 7.94% to 31.31%. PNA% provides a direct insight into n-alkanes from petrogenic sources. In this study, PNA% was 83±4.41%, implying that 83% of n-alkanes were originated from anthropogenic sources. The ACL value varied from 27.45 to 30.95, which was consistent with the calculated result (29.2±0.8) of Delhi in India (Yadav et al., 2013). This small fluctuations may suggest that n-alkanes emissions were similar across different sampling sites, displayed a relative homogeneous distribution in Jiujiang.

**3.1.3 Hopanes and steranes**

Hopanes and steranes are usually found in crude oil and engine oil, subsequently in vehicle exhausts from unburned lubricating oil residues. They are regarded as markers of fossil fuel combustion. The concentration profile of hopanes and alkanes was shown in Fig. 3c. Their total concentrations ranged from 1.1 to 20.5 ng $m^{-3}$, and the concentration of hopanes was approximately two times of that of steranes. As expected, the total concentrations of hopanes/steranes were 6.7/2.5, 3.3/1.2 and 1.9/1.1 ng $m^{-3}$ in petrochemical industry (SH), traffic area (SL) and suburban area (WQ), respectively.

The predominant hopane analogs were $C_{30}$–αβ–H (αβ–Hopane), $C_{31}$–αβ–S (ab 22S–Homohopane) and $C_{29}$–αβ– NOR–H (αβ–Nnorhopane), with concentrations of 1.2±1.3, 0.8±0.7 and 0.8±0.9 ng $m^{-3}$, respectively. The homohopane index ($C_{31}$–S/(S+R)) was 0.75, much greater than those of diesel (0.49), gasoline vehicle emissions (0.50–0.62) and petroleum

(0.6), but a bit smaller than industrial bitumite coal (0.87) (Fraser et al., 2002). This implies vehicle exhausts, petrochemical emissions and coal combustion have all contributed to particle concentrations. The concentration profiles of steranes were similar at different sites, with ααα–20R–EC (ααα–20R24R–Ethylcholestane) being the most abundant, followed by ααα–20R–C (ααα–20R Cholestane). This pattern was a bit different from that in Delhi which was dominated by $C_{29}$ sterane (Yadav et al., 2013).

### 3.2 Size-specific distributions

Particulate matters within 13 size fractions were collected. The size-specific distribution of NPOCs was then obtained (Fig. 4). The mean $\Sigma_{15}$PAHs (Fig. 4a) in each size fraction ranged from 0.4 ng $m^{-3}$ in the 0.01–0.018 μm fraction to 5.1 ng $m^{-3}$ in the 0.56–1.00 μm fraction. A bimodal distribution of the concentrations of PAHs was observed, with peaks in 0.56–1.00 and 9.90–18.0 μm fractions, respectively. PAHs in the 0.56–1.00 μm fraction were the most abundant. This phenomenon could be reasonably explained by that heavy molecular weight PAHs tend to be enriched in smaller particles (< 1.4 μm) (Kleeman et al., 2008), which generally originates from gas-particle transformation, adsorption of gaseous PAHs by condensation or coagulation of combustion products on the surface of preexsiting particles. However, the light molecular weight PAHs are speculated to adsorbed onto coarse particles, mainly originated from resuspension of soil or dust, plant tissue and growing particles from small diameters. As discussed above, the heavy molecular weight PAHs (>4– ring) accounted for 33.7–73.7% (mean of 50.6%) of the total PAHs, and the MDRs values of PAHs species, both confirmed our deduce that the condensation or coagulation of combustion products contributed to the size distribution pattern of PAHs. Similarly, Hien et al. (2007) found that PAHs accumulated predominantly in small size fractions (especially < 0.4 μm) in urban aerosols. More recently, Mu et al. (2017) indicated PAHs were strongly correlated with accumulation mode particles (0.05–2.0 μm), and PAHs in this fraction accounted for ~85% of the total measured PAHs.

The concentrations of n-alkanes (Fig. 4b) in Aitken nuclei (<0.05 μm), Accumulation and Coarse mode (>2.0 μm) particles were 1.7–3.1, 7.0–28.7 and 4.7–6.3 ng $m^{-3}$, respectively. The concentrations of n-alkanes in individual fractions accounted for 1.5–24.5% of the total measured n-alkanes in all fractions. n-Alkanes in the 0.56–1.00 μm fraction were the most abundant, whereas n-alkanes in three nano-size fractions accounted for the smallest percentages (1.5–2.5%). Notably, the concentration of n-alkanes increased with increase in fraction size. After fraction size reached 1.00 μm, however, the concentration of n-alkanes decreased in coarse mode particles. This implies n-alkanes have a tendency to be adsorbed on fine particles. In general, condensation is more likely happen to fine particles because of their large quantity and larger specific surface area (Wang et al., 2009).

The size-specific distribution of hopanes and steranes was illustrated in Fig. 4c. Hopanes and steranes were the most

abundant in the following five fractions: 0.56–1.00 μm (2.9 ng $m^{-3}$), 0.32–0.56 μm (2.5 ng $m^{-3}$), 0.18–0.32 μm (1.8 ng $m^{-3}$), 9.9–18 μm (1.2 ng $m^{-3}$) and 0.10–0.18 μm (1.1 ng $m^{-3}$). Approximately 55% of ∑(hopanes+steranes) were associated with the 0.10–1.00 μm fraction, which probably was due to their origins from fossil fuel combustion. This result was consistent with that of Kleeman et al. (2008) who found the hopanes and steranes were abundant in ultrafine size fraction during a severe winter pollution episode in Sacramento, USA.

Moreover, our recent research (Han et al., 2018) found that the organic compounds carrier, OC/EC, displayed a unimodal distribution in the fraction of 0.56–1.0 μm among the 13– staged particles. It is also suggested that EC could provide adsorption sites for organic compounds (e.g. NPOCs) due to its large surface area, and has the catalytic properties for redox chemistry reactions. In fact, the relationship between the concentration of NPOCs and the size particles is highly variable. This suggests not only source type but also photodegradation and gas-particle partitioning have great influences on the size-specific distribution of NPOCs, which would be further discussed in Section 3.3 and Section 3.4, respectively.

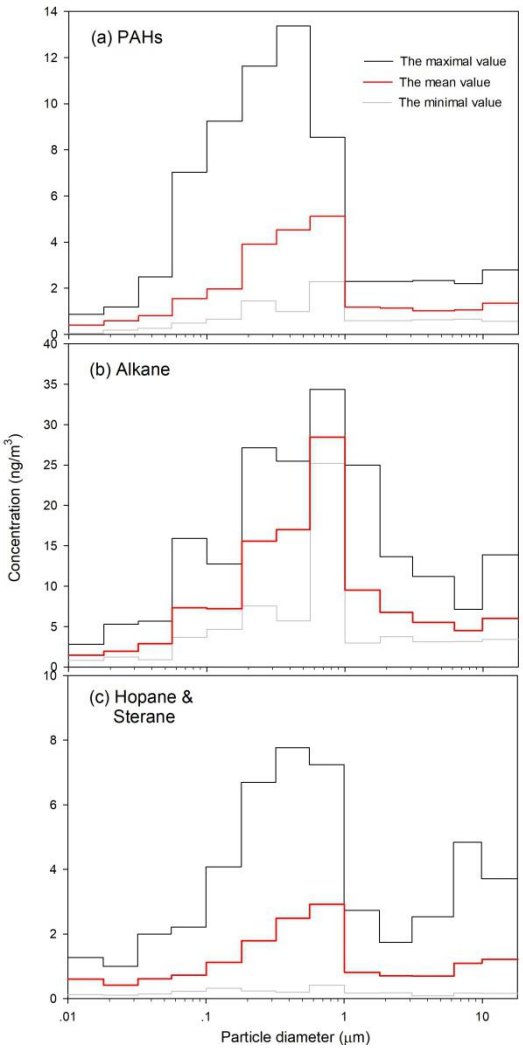


**Fig. 4.** Mean-normalized size-specific distribution of NPOCs in the collected $PM_{2.5}$ samples

### 3.3 Degradation of organics

Photochemical oxidation has great influences on the mass concentration and size-specific distribution of NPOCs, and on their removal and atmospheric fate (May et al., 2012). Photochemical decay could cause the ambient data to be distributed along a line emanating from the source profile in ratio–ratio plot, with increasing photochemical age (Robinson et al., 2006;Yu et al. 2011). EC shares common origins with PAHs and hopanes but they are subject to photodegradation. In this study, two pairs of EC normalized PAHs and hopanes (Fig. 5), namely IcdP/BghiP and C29–αβ–NOR/C30–αβ–H (αβ–Nnorhopane/αβ–Hopane), were adopted to visually compare the distributions of critical marker species and investigate explore the degradation of NPOCs (Robinson et al., 2006;Wang et al., 2016).

Most of the EC normalized IcdP/BghiP data points were distributed along a line (Fig. 5a), implying ambient PAHs underwent photochemical degradation and influenced by vehicle emissions and coal combustion. It was reported that the free ends of C-C scission products of PAHs remain tethered together, which prevent fragmentation and help forming more functional group from the reactions with OH· radical (Hunter et al., 2014). Ultimately, forming the low volatility species which can condense on the particle phase. There were several deviation points at left down corner, and the values were smaller than the values of tunnel and vehicle source profile, indicating mixed influence from traffic origins and degradation. Yu et al. (2011) reported a more apparent liner distributions of data sets measured in Hong Kong and PRD, which can be attributed to their single vehicle source type.

In Fig. 5b, most of the data were linearly distributed, implying the photochemical decay of C29–αβ–NOR/C30–αβ–H in this study. Previous research provided evidences that photochemical oxidation alters the molecular-level composition of hopanes (Robinson et al., 2006). OH· radical was expected to the major atmospheric oxidants, and rudimentary calculations suggest that OH· oxidized hopanes on time scale of a few days which depended on aerosol size. Moreover, the C29–αβ–NOR/C30–αβ–H ratio–ratio plot also suggests both biomass burning and vehicle emission contributed to hopanes concentrations in this study. Robinson et al. (2006) found hopanes were severely depleted in Pittsburgh, USA, and they attributed this phenomenon to regional air mass transport affecting the oxidation of condensed-phase organic compounds.

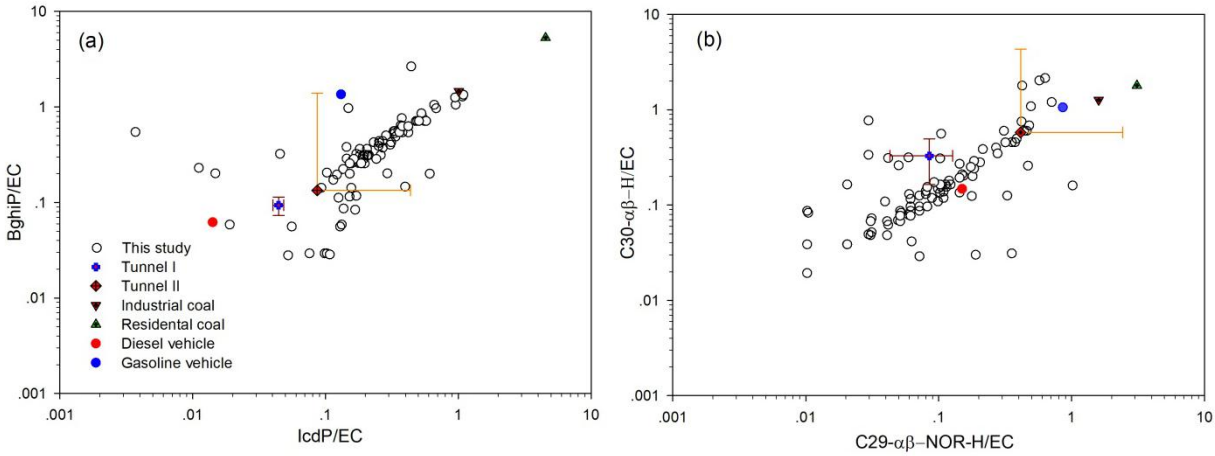


394

395 **Fig. 5.** Ratio–ratio plots of two pairs of characterized species (IcdP/BghiP and C29–αβ–NOR–H/C30–αβ–H)
396 normalized by EC and published source profiles. **(**Tunnel I: Yu et al., 2011; Tunnel II: He et al., 2009; Residental
397 coal: Zhang et al., 2008; Industrial coal: Zhang et al., 2008; Diesel vehicle: Fraser et al., 2002; Gasoline vehicle:
398 Fraser et al., 2002**)**

399 **3.4 Impact of gas-particle partitioning on fine particle source apportionment**

400 **3.4.1 Gas-particle partitioning**

401 An important aspect of atmospheric NPOCs is their gas-particle partitioning behavior, which has effects on their fate and
402 size-specific occurrence. The particle-phase fraction (φ) of NPOCs was calculated according to gas-particle partitioning
403 model (Fig. 6 and Fig. S2-S3). The gas-phase fractions of LMW PAHs (e.g., FLO, PHE, ANT, FLU and PYR) were
404 rather substantial, and their particle-phase fractions (φ) ranged from 2.4% to 51.3%. Similarly, the φ values of short chain
405 $C_{22}$–$C_{24}$ n-alkanes varied between 21.2% and 62.5%, exhibiting an increasing trend with increase in their molecular
406 weight. However, for the heavier molecular weight species, the φ values remained greater than 90.0% for all temperature
407 ranges. The calculated φ values of PAHs and n-alkanes were comparable to those estimated in urban Denver, Chicago
408 and Los Angeles in USA (Xie et al., 2013), but a bit greater than those in PRD of China (Wang et al., 2016). The lower
409 fractions of NPOCs in gas phase in this study compared with that in PRD was probably because PRD area is located in a
410 border region between subtropics and tropics. PRD has higher temperature than Eastern China area, especially in cold
411 winter seasons, and the higher temperature can facilitate the shift of species to gas phase.

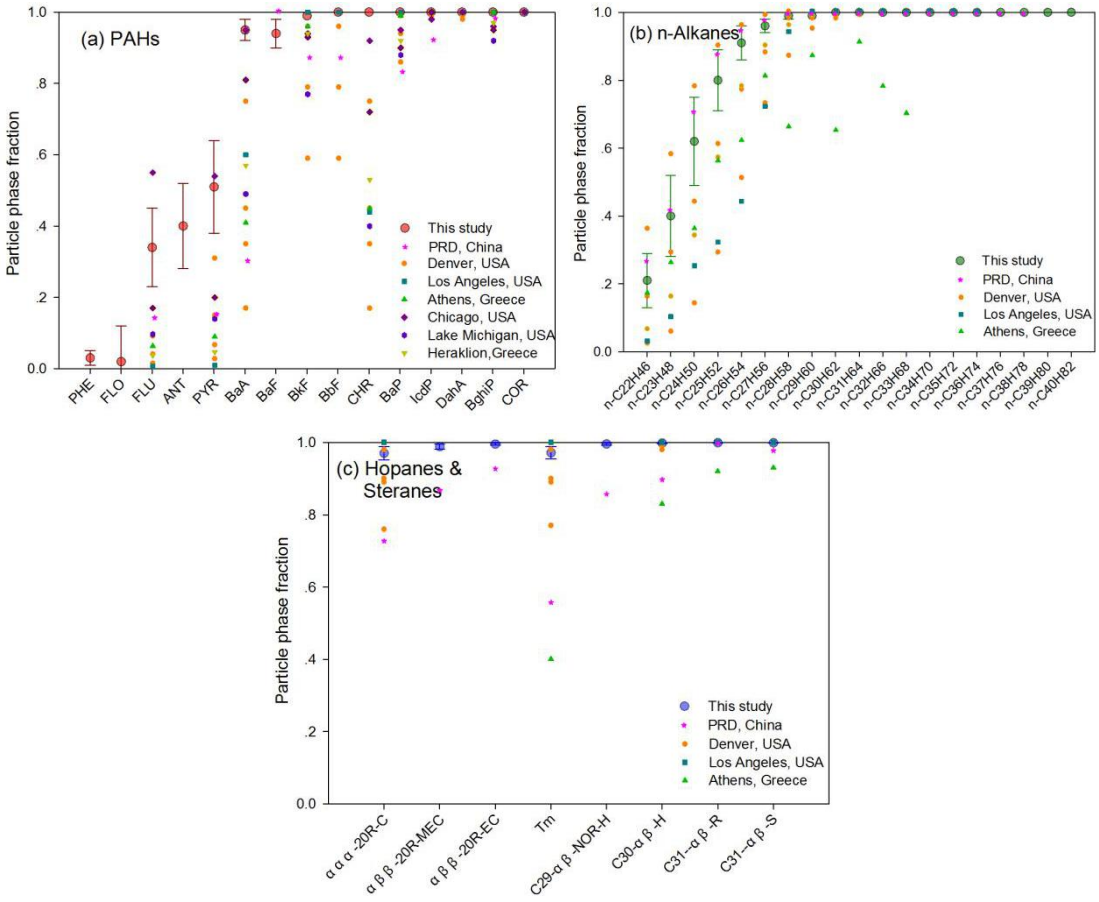


**Fig. 6.** Average particle-phase fractions (φ) of all NPOCs as in comparison with previous results

### 3.4.2 PMF source apportionment

Source apportionment analysis involves techniques that can be used to identify source species and their unique contributions, which are critical in making policies of controlling pollution. It is typically assumed the molecular markers are stable in the ambient environment, *i.e.*, being nonreactive and nonvolatile (May et al., 2012). However, as discussed above, many organic markers can be oxidized over atmospherically relevant time scales, and partition between gas and particle phases. If the data of NPOCs in single particle phase are directly used as input for receptor model, this may confound the aerosol factors.

Additionally, individual organic tracers, elemental species, inorganic ions and OC/EC have been demonstrated to be able to provide source apportionment of aerosols. To explore the impact of gas-particle partitioning on $PM_{2.5}$ source apportionment, both single particle phase and the total (gas+ particle) NPOCs were incorporated with elemental species, inorganic ions and OC/EC, used as input data for receptor model PMF (detailed description about PMF model could be seen in Section S1 in Supplementary Materials). Results based on single particle phase and the total phases were denoted by $PMF_P$ and $PMF_T$, respectively. Five to eleven factors were extracted in this study to obtain reasonable results. Finally,

it turned out that the results of eight factors gave the most reasonable source profiles (Fig. 7 and Fig. S4).

Factor 1 (Fig. 7a) was characterized by significant presence of Al, Ca, Mg, Ti and Fe, which are regarded as good indicator of dust (including construction dust, geological dust and road dust) (Wang et al., 2015). These elements are the major elements of dust sand, usually accumulated in the coarse mode particles. Geological dust typically contains high concentrations of crustal elements, including Fe and Mn. Hence, this factor was regard as "dust", with percent contributions of 8.90% and 11.0% under $PMF_P$ and $PMF_T$, respectively.

Factor 2 (Fig. 7b) was characterized by the significant presence of Cu, Mn, Zn, Pb, BkF, BbF, BaF and BaP. Mn, Zn and As are related to emissions from steel production, brick, ceramic and glass making factories (Li et al., 2016;Sulong et al., 2017). Cu mainly originates from non-ferrous metal production and smelting factories. BkF, BbF and BaP are typical markers of emissions from coke industry. Several large-scale industrial parks are located in Jiujiang city, e.g., Shacheng Industry and Jiujiang Comprehensive Industry in the northern and southern areas, respectively. Therefore, factor 2 was associated with industrial emission.

Factor 3 (Fig. 7c) was characterized by large fractions of HMW PAHs (IcdP, BghiP, DahA and COR), as well as relatively high fractions of hopanes and steranes. BghiP and COR are excellent tracers of vehicle exhausts. Hopanes and steranes are related to exhausts from heavy-duty vehicles with diesel engines(Wang et al., 2016). As mentioned above, there were over 700 thousand motor vehicles in Jiujiang city in 2015, among which about 1/15 were mainly powered by diesel engines. Therefore, factor 3 was identified as "vehicle related exhausts", with percent contributions of 12.5% and 15.0% under $PMF_P$ and $PMF_T$, respectively.

Factor 4 (Fig. 7d) was characterized by the presence of well-documented indicators of secondary aerosol formation, such as $NO_3^-$, $SO_4^{2-}$ and $NH_4^+$, with factor fractions of 83.7%, 87.4% and 94.1%, respectively. These secondary products are formed by precursor gases ($SO_2$ and NOx) via oxidation reactions(Wang et al., 2015). They are mainly emitted from biomass burning, coal combustion and vehicles. $NO_3^-$, $SO_4^{2-}$ and $NH_4^+$ accounted for 19.9–22.3%, 16.4–18.1% and 10.4–13.7% of $PM_{2.5}$ concentrations, respectively, which were typically derived from gas-particle conversion process as well as homogeneous and heterogeneous reactions in urban atmosphere. Furthermore, the similar spatial distribution and contribution in all sites highlight a widespread of these components. Consequently, factor 4 was identified as "secondary aerosol formation".

Factor 5 (Fig. 7e) was characterized by significant presence of $C_{30}$–$C_{40}$ n–alkanes, as well as relatively significant presence of FLU and PYR. In previous research (Wang et al., 2016), the long chain n–alkanes ($C_{29}$–$C_{36}$) were considered to come from local emissions, especially from coal combustion. PYR and FLU are frequently considered as excellent markers of coal combustion for aerosol source apportionment. Coal is the primary energy source for many industries in

458 China. About 3.1 million tons of standard coal are consumed per year by the Jiujiang thermal power plant according to
459 local statistics. Thus, factor 5 was identified as “coal burning”, with percent contributions of 18.7% and 16.4% under
460 $PMF_P$ and $PMF_T$, respectively.
461 Factor 6 (Fig. 7f) was characterized by high percentage of $Cl^-$ and $K^+$, with some amounts of As, Se, Pb, OC and EC. $Cl^-$
462 and $K^+$ have been widely used as tracers of wood and biomass burning aerosol (Li et al., 2016). In the past, crop straws
463 were disposed bu local farmers in the field by burning for convenience. Although this has been extensively banned in
464 recent years, several large-scale straw burning sites surrounding this city can still be observed by China National Satellite
465 Meteorological Center (http://hjj.mep.gov.cn/jgjs/). Thus, this factor was considered as “biomass burning”, with percent
466 contributions of 12.7% and 15.7% under $PMF_P$ and $PMF_T$, respectively.
467 Factor 7 (Fig. 7g) was characterized by high fraction of Ni and V, which are excellent tracers of exhausts from ship and
468 heavy-duty diesel vehicles. In fact, Jiujiang harbor is among the ten busiest harbors in Yangtze River, whose port cargo
469 throughput is 59 million tons per year. Hence, factor 7 was identified as “shipping and diesel exhausts”.
470 Factor 8 (Fig. 7h) was characterized by a high load of short chain n–alkanes ($C_{22}H_{46}$, 76.6%; $C_{23}H_{48}$, 84.2%; $C_{24}H_{50}$,
471 81.1%) and LMW PAHs (about 60% for FLU, PYR, BaA and CHR). These species have several characteristics: most of
472 their particle-phase fractions (φ) were less than 50%; relatively light molecular weight; strongly temperature-dependent
473 vaporization. These compounds have been interpreted as “light NPOCs factor” in previous research (Xie et al.,
474 2013;Wang et al., 2016). The percent contributions of this factor were 3.7% and 5.6% under $PMF_P$ and $PMF_T$,
475 respectively. Additionally, concentrations of light NPOCs factor showed an increasing trend with increase in temperature,
476 implying the association of this factor with fossil fuel evaporation and biogenic emissions. Hence, this factor was
477 regarded as “light NPOCs factor”.

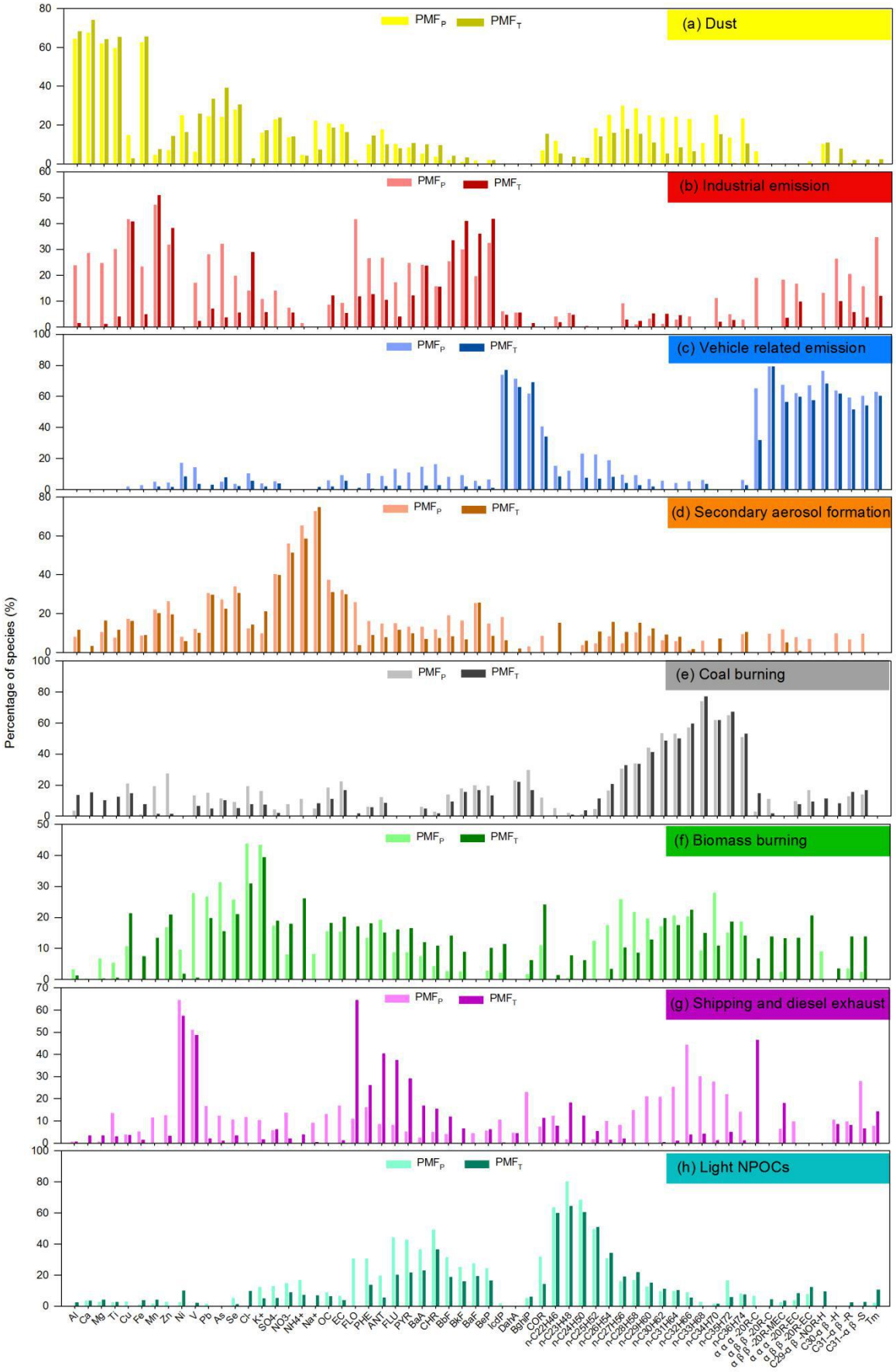


**Fig. 7.** Source profiles of eight sources resolved by PMF

480 **3.4.3 Assessing impacts of gas-particle partitioning on source apportionment**

481 As stated above, using the data of single particle phase as input data for PMF model could lead to uncertainty in results,
482 which was related to gas-particle partitioning of NPOCs in the mathematical solution. This influence could be reduced
483 via adding the predicted gaseous NPOCs concentrations when the measured gaseous NOCs data were not available. In
484 the present study, the eight extracted factors showed similar source profiles between $PMF_P$ and $PMF_T$, which was in
485 sharp contrast with one recent research that found several very volatile NPOCs (like FLU) were quite variable in $PMF_T$,
486 but almost did not appear in $PMF_P$ in PRD (Wang et al., 2016). This difference could probably be due to the $PM_{2.5}$ source
487 identification in this study was focused on the period of high-frequency haze episodes (late autumn and winter), the
488 major predicted NPOCs compounds enriched in particle phase. While the NPOCs investigation conducted in PRD
489 included hot summer season, which would enhanced the uncertainty and variability of predicted light NPOCs.
490 Despite the current study could not predict gas-phase NPOCs with high accuracy, the source apportionment result
491 extracted by $PMF_P$ and $PMF_T$ were comparable. Using the data of total organic compounds in gas-particle phases with
492 other aerosol species as input data for receptor model, provides an excellent tool for $PM_{2.5}$ source apportionment.
493 However, due to the uncertainty of $MW_{OM}$, $\xi_{OM}$ and $P^o_L$ values, the gaseous phase light NPOCs might be overestimated,
494 especially for light NPOCs. Hence, reasonable caution should still be given to the more volatile organic species.

495 **3.5 Limitation and implication**

496 In this work, we confirmed that using the total (gas+ particle) NPOCs as input data for receptor model provides a better
497 source apportionment than using only particle phase. However, the predicted gas NPOCs from gas-particle partitioning
498 may bring some uncertainty. For example, the partitioning process are strongly affected by the particle properties
499 (particle size, organic carbon compounds), photodegradation and the prevailing ambient temperature. For
500 size-distribution, the $PM_{2.5}$ associated NPOCs in the 0.56–1.00 μm fraction were the most abundant, our recent study also
501 found OC was primarily distributed in this fraction (Han et al., 2018). Abundant OC would adsorb/absorb large amounts
502 of NPOCs, resulting particle bound NPOCs concentration increasing in this particle size. While gas phase oxidation
503 reaction is much faster than heterogeneous reactions in aerosol surface, since the uptake of heterogeneous oxidant is
504 diffusion-limited (Robinson et al., 2006;May et al., 2012).
505 Low temperature promotes NPOCs adsorbing/absorbing onto aerosols, while photochemical degradation of NPOCs is
506 relatively weak in cold season. Moreover, photochemical reactions would reduce the abundances of organic marker
507 depend on species, significantly altering the relative contribution of different sources extracted by liner source inversion.
508 Compared with long time investigation, this study was mainly focused in cold season, which would lead to relative high

509 abundance of particle NPOCs with small variation.

510 For PMF model, it has limit that could not identify potential source without preexisting tracer. Also, the relative small
511 number of measurements might lead to some uncertainty in source apportionment. In the future, more source tracers data
512 need to be included for the calculation of potential contributions.

513 **4. Conclusions**

514 NPOCs are typical molecular markers for source identification, which attract researchers' interest worldwide. Fifty-seven
515 $PM_{2.5}$-associated NPOCs including PAHs, n–alkanes, iso–alkanes, hopanes and steranes were identified and quantified
516 using a TD–GC/MS method in a typical city in Eastern China. The total concentrations of NPOCs were 31.7–388.7 ng
517 $m^{-3}$, with n-alkanes being the most abundant species (67.2%). The heavy molecular weight PAHs (4- and 5-ring)
518 contributed 67.9% of the total PAHs, and the middle chain length ($C_{25}$–$C_{34}$) n-alkanes were the most abundant in
519 n-alkanes.

520 For size distribution, PAHs and n-alkanes were majorly enriched in 0.56–1.00 μm fraction, and ∑(hopanes+steranes)
521 were associated with 0.32–1.00 μm fraction, implying their similar source of combustion products. The ratio–ratio plots
522 of IcdP/BghiP and C29–αβ–NOR/C30–αβ–H implied that NPOCs in local area were affected by photochemical
523 degradation. Using single particle ($PMF_P$) and total (particle+ gas, $PMF_T$) phases NPOCs as input data for PMF model,
524 respectively, we successfully extracted eight factors from both cases. The $PMF_T$ showed better source profiles than $PMF_P$,
525 and the light NPOCs factor contributed a bit more in $PMF_T$ (5.6%) than in $PMF_P$ (3.7%). This study indicates that NPOCs
526 are useful for aerosol apportionment, and total NPOCs in two phases enable better source profiles than NPOCs in single
527 particle phase.

528 **Acknowledgement**

529 This study was financially supported by National Natural Science Foundation of China (No. 21577090 and No.21777094)
530 and Jiujiang Committee of Science and Technology (Grant No. JXTCJJ2016130099). We thank Jiujiang Environmental
531 Protection Agency and Jiujiang Environmental Monitor Station for coordinating the sampling process and for their
532 valuable contribution to field measurement. We appreciate senior engineer Yajuan Zhou (Instrumental Analysis Center,
533 Shanghai Jiao Tong University) for her assistance in experimental analysis.

534 **References**


535 And, J. S. C., and Hanshaw, W.: Vapor Pressures and Vaporization Enthalpies of the n-Alkanes from C31 to C38 at T =
536 298.15 K by Correlation Gas Chromatography, J. Chem. Engineering Data, 49, 620-630, 2004.

537 Chen, P., Li, C., Kang, S., Rupakheti, M., Panday, A. K., and Zhang, Q.: Polycyclic aromatic hydrocarbons (PAHs) in
538 aerosols over the central Himalayas along two south-north transects, Atmos. Chem. Phys., 18, 1-38, 2016a.

539 Chen, X., Balasubramanian, R., Zhu, Q., Behera, S. N., Bo, D., Huang, X., Xie, H., and Cheng, J.: Characteristics of
540 atmospheric particulate mercury in size-fractionated particles during haze days in Shanghai, Atmos. Environ., 131,
541 400-408, 2016b.

542 Ding, L. C., Ke, F., Wang, D. K. W., Dann, T., and Austin, C. C.: A new direct thermal desorption-GC/MS method:
543 Organic speciation of ambient particulate matter collected in Golden, BC, Atmos. Environ., 43, 4894-4902, 2009.

544 Feng, J., Hu, M., Chan, C. K., Lau, P. S., Fang, M., He, L., and Tang, X.: A comparative study of the organic matter in
545 $PM_{2.5}$ from three Chinese megacities in three different climatic zones, Atmos. Environ., 40, 3983-3994, 2006.

546 Fraser, M. P., Lakshmanan, K., Fritz, S. G., and Ubanwa, B.: Variation in composition of fine particulate emissions from
547 heavy-duty diesel vehicles, J. Geophys. Res. Atmos., 107, ICC 8-1-ICC 8-6, 2002.

548 Han, D., Zhang, J., Hu, Z., Ma, Y., Duan, Y., Han, Y., and Cheng J.: Particulate mercury in ambient air in Shanghai,
549 China: Size-specific distribution, gas-particle partitioning, and association with carbonaceous composition. Environ.
550 Pollut., 238, 543-553, 2018.

551 Hao, Y., and Liu, Y. M.: The influential factors of urban PM 2.5 concentrations in China: aspatial econometric analysis, J.
552 Cleaner Production, 112, 1443-1453, 2015.

553 He, J., and Balasubramanian, R.: A study of gas/particle partitioning of SVOCs in the tropical atmosphere of Southeast
554 Asia, Atmos. Environ., 43, 4424-4434, 2009.

555 Hien, T. T., Le, T. T., Kameda, T., Takenaka, N., and Bandow, H.: Distribution characteristics of polycyclic aromatic
556 hydrocarbons with particle size in urban aerosols at the roadside in Ho Chi Minh City, Vietnam, Atmos. Environ., 41,
557 1575-1586, 2007.

558 Ho, S. S., and Yu, J. Z.: In-injection port thermal desorption and subsequent gas chromatography-mass spectrometric
559 analysis of polycyclic aromatic hydrocarbons and n-alkanes in atmospheric aerosol samples, J. Chromatography A, 1059,
560 121, 2004.

561 Ho, S. S. H., Yu, J. Z., Chow, J. C., Zielinska, B., Watson, J. G., Sit, E. H. L., and Schauer, J. J.: Evaluation of an
562 in-injection port thermal desorption-gas chromatography/mass spectrometry method for analysis of non-polar organic

563 compounds in ambient aerosol samples, J. Chromatography A, 1200, 217-227, 2008.
564 He, L. Y., Hu, M., Zhang, Y. H., Huang, X. F., Yao, T. T.: Fine particle emissions from on-road vehicles in the Zhujiang
565 tunnel, China. Environ. Sci. Technol., 42(12), 4461-4466, 2008.
566 Huang, R. J., Zhang, Y., Bozzetti, C., Ho, K. F., Cao, J. J., Han, Y., Daellenbach, K. R., Slowik, J. G., Platt, S. M., and
567 Canonaco, F.: High secondary aerosol contribution to particulate pollution during haze events in China, Nature, 514, 218,
568 2014.
569 Huang, X., Liu, Z., Liu, J., Hu, B., Wen, T., Tang, G., Zhang, J., Wu, F., Ji, D., and Wang, L.: Chemical characterization
570 and synergetic source apportionment of $PM_{2.5}$ at multiple sites in the Beijing–Tianjin–Hebei region, China, Atmos. Chem.
571 Phys.,1-34, 2017.
572 Hunter, J. F., Carrasquillo, A. J., Daumit, K. E., Kroll, J. H.: Secondary organic aerosol formation from acyclic,
573 monocyclic, and polycyclic alkanes. Environ. Sci. Technol., 48(17), 10227-34, 2014.
574 Kim, D. G., Choi, K. I., and Lee, D. H.: Gas-particle partitioning and behavior of dioxin-like PCBs in the urban
575 atmosphere of Gyeonggi-do, South Korea, Atmos. Res., 101, 386-395, 2011.
576 Kleeman, M. J., Riddle, S. G., and Jakober, C. A.: Size distribution of particle-phase molecular markers during a severe
577 winter pollution episode, Environ. Sci. Technol., 42, 6469-6475, 2008.
578 Kuang, Y. W., Huang, Z. H., Wen, D. Z., Li, J., and Huang, L. B.: Unravelling airborne polycyclic aromatic hydrocarbons
579 (PAHs) in southern China using tree-rings of 100-yr old Pinus Kwangtungensis, Atmos. Chem. Phys. Discussions, 11,
580 27359-27382, 2011.
581 Li, J., Wang, G., Ren, Y., Wang, J., Wu, C., Han, Y., Zhang, L., Cheng, C., and Meng, J.: Identification of chemical
582 compositions and sources of atmospheric aerosols in Xi'an, inland China during two types of haze events, Sci. Total
583 Environ., 566-567, 230, 2016.
584 Li, L., Tan, Q., Zhang, Y., Feng, M., Qu, Y., An, J., and Liu, X.: Characteristics and source apportionment of $PM_{2.5}$ during
585 persistent extreme haze events in Chengdu, southwest China, Environ. Pollution, 230, 718, 2017.
586 Li, Y. C., Yu, J. Z., Ho, S., Schauer, J. J., Yuan, Z. B., Lau, A. K. H., and Louie, P. K. K.: Chemical characteristics and
587 source apportionment of fine particulate organic carbon in Hong Kong during high particulate matter episodes in winter
588 2003, Atmos. Res., 120–121, 88-98, 2013.
589 Ma, W. L., Sun, D. Z., Shen, W. G., Yang, M., Qi, H., Liu, L. Y., Shen, J. M., and Li, Y. F.: Atmospheric concentrations,
590 sources and gas-particle partitioning of PAHs in Beijing after the 29th Olympic Games, Environ. Pollution, 159,
591 1794-1801, 2011.
592 Ma Y., Dai H., Li L., Chen C., Sun Q, Fan J., Li Y., Huang T.: A rapid method for screening on organic pollutants in

$PM_{2.5}$ using GCMS combined with compound composer software, Environ. Chem. 37(1), 188-191, 2018.

May, A. A., Saleh, R., Hennigan, C. J., Donahue, N. M., and Robinson, A. L.: Volatility of organic molecular markers used for source apportionment analysis: measurements and implications for atmospheric lifetime, Environ. Sci. Technol., 46, 12435, 2012.

Mu, L., Peng, L., Liu, X., He Q., Bai, H., Yan,Y., Li Y.: Emission characteristics and size distribution of polycyclic aromatic hydrocarbons from coke production in China, Atmos. Res., 197, 113-120, 2017.

Okonski, K., Degrendele, C., Melymuk, L., Landlová, L., Kukučka, P., Vojta, Š., Kohoutek, J., Čupr, P., and Klánová, J.: Particle Size Distribution of Halogenated Flame Retardants and Implications for Atmospheric Deposition and Transport, Environ. Sci. Technol., 48, 14426-14434, 2014.

Pankow, J. F.: An absorption model of the gas/aerosol partitioning involved in the formation of secondary organic compounds, Atmos. Environ., 28, 189-193, 1994.

Rajput, P., and Sarin, M. M.: Polar and non-polar organic aerosols from large-scale agricultural-waste burning emissions in Northern India: Implications to organic mass-to-organic carbon ratio, Chemosphere, 103, 74-79, 2014.

Robinson, A. L., Donahue, N. M., and Rogge, W. F.: Photochemical oxidation and changes in molecular composition of organic aerosol in the regional context, J. Geophy. Res. Atmos., 111, 375-402, 2006.

Rogge W F, Hildemann L M, Mazurek M A.: Sources of fine organic aerosol. 6. Cigaret smoke in the urban atmosphere. Environ. Sci. Technol., 28(7):1375-88, 1994.

Shen, X. J., Sun, J. Y., Zhang, X. Y., Zhang, Y. M., Zhang, L., Che, H. C., Ma, Q. L., Yu, X. M., Yue, Y., and Zhang, Y. W.: Characterization of submicron aerosols and effect on visibility during a severe haze-fog episode in Yangtze River Delta, China, Atmos. Environ., 120, 307-316, 2015.

Sulong, N. A., Latif, M. T., Khan, M. F., Amil, N., Ashfold, M. J., Mia, W., Chan, K. M., and Sahani, M.: Source apportionment and health risk assessment among specific age groups during haze and non-haze episodes in Kuala Lumpur, Malaysia, Sci. Total Environ., 601–602, 556-570, 2017.

Wang, G., Kawamura, K., Xie, M., and Hu, S.: Size-distributions of n-hydrocarbons, PAHs and hopanes and their sources in the urban, mountain and marine atmospheres over East Asia, Atmos. Chemi. Phys. Discussions, 9, 8869-8882, 2009.

Wang, G., Kawamura, K., Xie, M., Hu, S., Gao, S., Cao, J., An, Z., Wang, Z.: Size-distributions of n-alkanes, PAHs and hopanes and their sources in the urban, mountain and marine atmospheres over East Asia. Atmos. Chem. Phy. 9, 8869-8882, 2009.

Wang, Q., Zhuang, G., Huang, K., Liu, T., Deng, C., Xu, J., Lin, Y., Guo, Z., Chen, Y., and Fu, Q.: Probing the severe haze pollution in three typical regions of China: Characteristics, sources and regional impacts, Atmos. Environ., 120,

623 76-88, 2015.
624 Wang, Q., Feng, Y., Huang, X. H. H., Griffith, S. M., Zhang, T., Zhang, Q., Wu, D., and Yu, J. Z.: Non-polar organic
625 compounds as PM2.5 source tracers: Investigation of their sources and degradation in the Pearl River Delta, China, J.
626 Geophy. Res. Atmos, 2016.
627 Xie, M., Barsanti, K. C., Hannigan, M. P., Dutton, S. J., and Vedal, S.: Positive matrix factorization of PM2.5 -
628 eliminating the effects of gas/particle partitioning of semivolatile organic compounds, Atmos. Chemi. Phys., 13, 7381,
629 2013.
630 Xie, M., Hannigan, M.P., Barsanti, K.C.: Impact of Gas/Particle Partitioning of Semivolatile Organic Compounds on
631 Source Apportionment with Positive Matrix Factorization. Environ. Sci. Technol. 48, 9053-9060, 2014.
632 Xie, Y., Ye, X., Ma, Z., Tao, Y., Wang, R., Zhang, C., Yang, X., Chen, J., and Chen, H.: Insight into winter haze formation
633 mechanisms based on aerosol hygroscopicity and effective density measurements, Atmos. Chemi. Phys., 17, 7277-7290,
634 2017.
635 Xu, H. M., Tao, J., Ho, S. S. H., Ho, K. F., Cao, J. J., Li, N., Chow, J. C., Wang, G. H., Han, Y. M., and Zhang, R. J.:
636 Characteristics of fine particulate non-polar organic compounds in Guangzhou during the 16th Asian Games:
637 Effectiveness of air pollution controls, Atmos. Environ., 76, 94-101, 2013.
638 Yadav, S., Tandon, A., and Attri, A. K.: Characterization of aerosol associated non-polar organic compounds using
639 TD-GC-MS: a four year study from Delhi, India, J. Hazard. Materials, 252–253, 29-44, 2013.
640 Yu, J. Z., Huang, X. H., Ho, S. S., and Bian, Q.: Nonpolar organic compounds in fine particles: quantification by thermal
641 desorption-GC/MS and evidence for their significant oxidation in ambient aerosols in Hong Kong, Analytical
642 Bioanalytical Chem., 401, 3125-3139, 2011.
643 Zhang, Y. L., Huang, R. J., El Haddad, I., Ho, K. F., Cao, J. J., Han, Y., Zotter, P., Bozzetti, C., Daellenbach, K. R., and
644 Canonaco, F.: Fossil vs. non-fossil sources of fine carbonaceous aerosols in four Chinese cities during the extreme winter
645 haze episode of 2013, Atmos. Chemi. Phys., 15, 1299-1312, 2015.
646 Zhao, Y., Zhang, Y., Fu, P., Ho, S. S., Ho, K. F., Liu, F., Zou, S., Wang, S., and Lai, S.: Non-polar organic compounds in
647 marine aerosols over the northern South China Sea: Influence of continental outflow, Chemosphere, 153, 332, 2016.
648